Available online at www.sciencedirect.com

jmr&t Journal of Materials Research and Technology

journal homepage: www.elsevier.com/locate/jmrt

Short Communication

Fabrication of the novel hybridized AZ31B Mg/CeO_2+ZrO_2 composites via multiple pass friction stir processing

Yongxin Li [a], *Olatunji Oladimeji Ojo* [b], *Sadeq Salman* [c], *Moslem Paidar* [d,*], *Mohamad Reda A. Refaai* [e], *Azlan Mohd Zain* [f], *Mahyuddin K.M. Nasution* [g], *Duqiang Xin* [h,**]

[a] *School of Computer Science, Xijing University, Xi'an, Shaanxi 710123, China*
[b] *Department of Industrial and Production Engineering, Federal University of Technology Akure, Nigeria*
[c] *Research Center, Al-Ayen University, Nasiriyah, Iraq*
[d] *Department of Materials Engineering, South Tehran Branch, Islamic Azad University, Tehran 1459853849, Iran*
[e] *Department of Mechanical Engineering, College of Engineering at Al Kharj, Prince Sattam Bin Abdulaziz University, Al Kharj 11942, Saudi Arabia*
[f] *Faculty of Computing, Universiti Teknologi Malaysia, 81310, Skudai, Johor, Malaysia*
[g] *Mathematics Study Program, FMIPA, Universitas Sumatera Utara, Medan 20155, Indonesia*
[h] *Shaanxi Engineering Research Center of Controllable NeutronSource, School of Electronic Information, Xijing University, Xi'an, 710123*

ARTICLE INFO

Article history:
Received 4 March 2023
Accepted 19 May 2023
Available online 23 May 2023

Keywords:
Multiple pass friction stir processing
Zirconium dioxide
Cerium oxide
Magnesium alloy
Mechanical properties
Corrosion

ABSTRACT

The mixture of the rare-earth CeO_2 and ZrO_2 particulates was used for fabricating the hybridized AZ31BMg/$(CeO_2+ZrO_2)_p$ composites by utilizing friction stir processing with a multiple-tool pass strategy. The structure, mechanical properties (tensile strength and hardness), tribological performances (wear properties) and corrosion behaviours of the hybrid composites were examined. The findings reveal the elimination of tunnel-like defects and clustering of the CeO_2+ZrO_2 particles in the composite after the multiple passes of the tool due to the successive mechanical stirring-assisted material flow. The rise in the tool passes reduced the mean grain sizes (7.91–3.02 μm), the particle sizes (5.47–2.28 μm), the average friction coefficient (0.45–0.18) and the specific wear rate (4.26×10^{-5} -2.17×10^{-5} mm^3/Nm) of the composite. The tensile strength (172–239 MPa), and the corrosion performance of the hybrid composite were also improved via the multiple tool pass strategy. Multiple tool pass is thus recommended for the fabrication of Mg-based hybrid composites.

* Corresponding author.
** Corresponding author.
E-mail addresses: m.paidar@srbiau.ac.ir (M. Paidar), xinduqiang@xijing.edu.cn (D. Xin).

https://doi.org/10.1016/j.jmrt.2023.05.170

1. Introduction

The structural application of magnesium alloys is limited owing to their major drawbacks such as low strength, poor mechanical integrity, and high corrosion and degradation rates [1]. Alkalization of electrolytes and H_2 evolution are also common outcomes of the degradation of Mg alloys [2]. It is thus important to have magnesium alloys with desirable and comprehensive properties. The simultaneous improvement in the mechanical and corrosion performance of magnesium (Mg) alloys can be accomplished by adding reinforcement particles

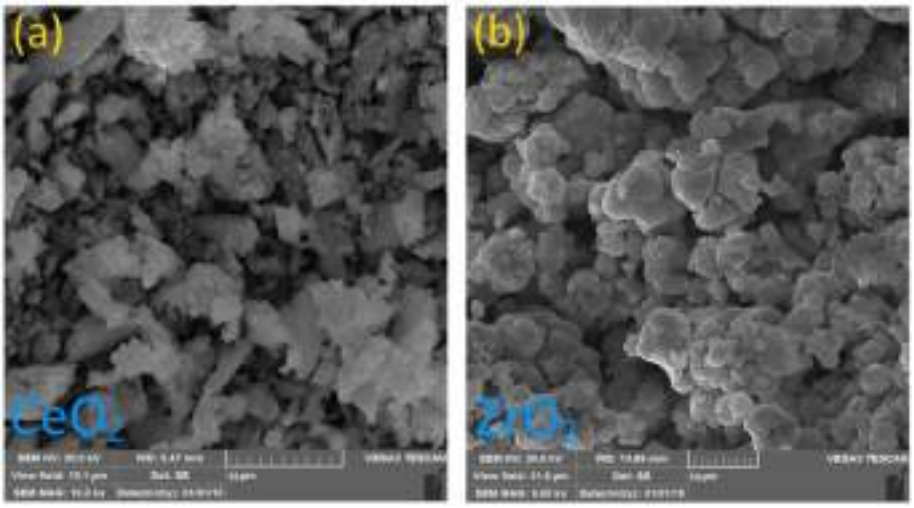

Fig. 1 – Secondary electron-SEM images of the reinforcements (a) CeO_2 and (b) ZrO_2.

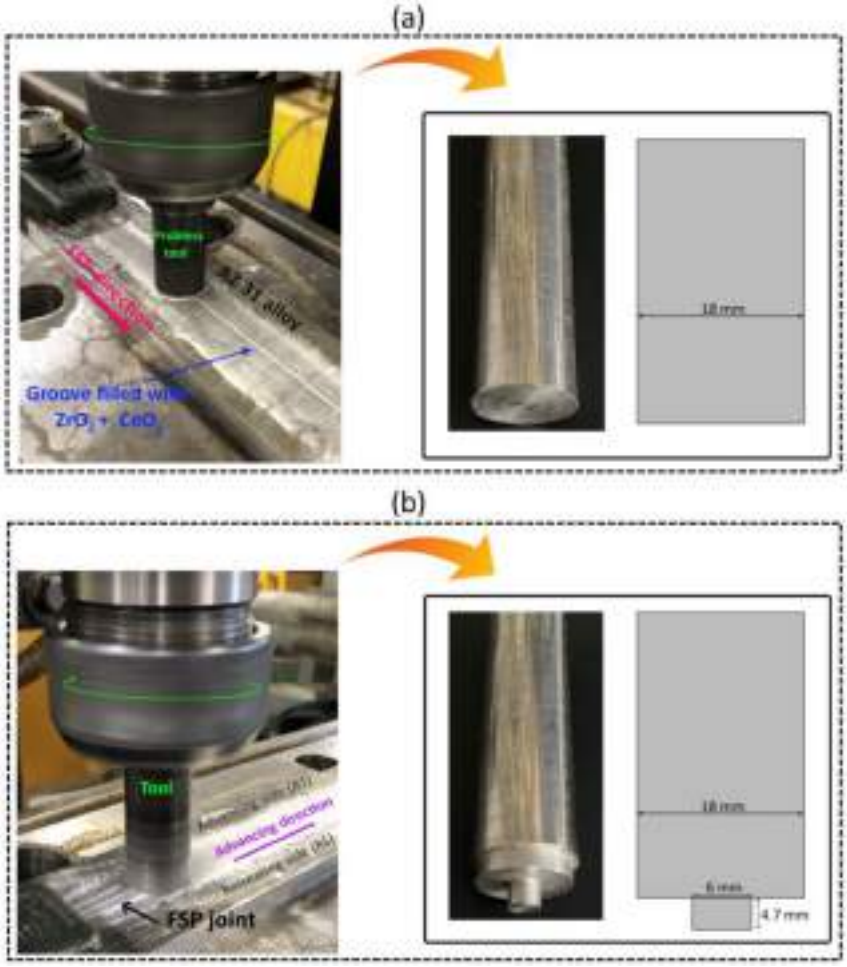

Fig. 2 – FSP of the hybridized composite (a) preliminary FSP processing with a pinless tool, (b) actual FSP processing.

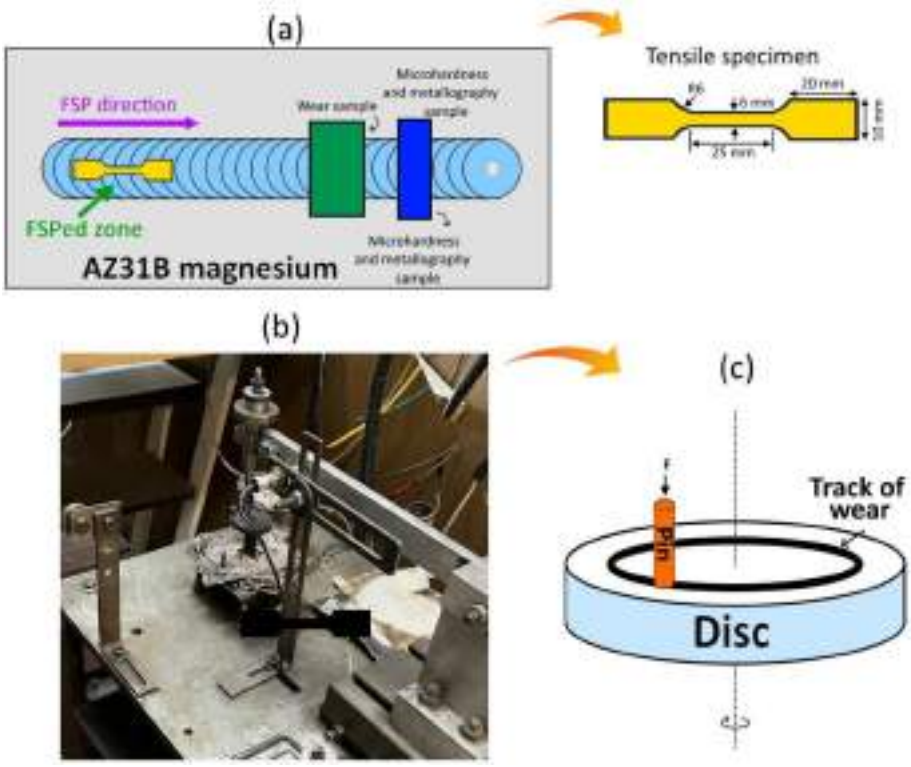

Fig. 3 – (a) Schematic showing test samples and dimensions of the tensile specimens, (b) wear testing, (c) schematic of wear test.

into Mg alloys. The methods for the development of Mg-based composites include stir casting and powder metallurgy. Unwanted defects such as uneven distribution of reinforced particles, solidification-induced defects, and cracks are common features of the Mg-based composites developed by the above-mentioned methods. These defects are stressed zones that diminish the strength-ductility of the developed composites. These challenges can be circumvented by employing severe plastic deformation processes like extrusion, rolling/multi-pass rolling/low-temperature rolling, and forging [3–5] but the processes are reckoned to be complicated and relatively ineffective. Presently, the solid-state friction stir processing technique is a better substitute for developing Mg-based composites as particle homogenization, grain refinement, and densification can be easily achieved [1,6]. The synergy of scattered dispersion of crystallographic texture and a high fraction of recrystallized grains (having high-angle grain boundaries) was acclaimed to have aided the improved strength-ductility properties of the FSP-processed AZ61 alloy [7].

Multi-pass friction stir processing has been identified as one of the ways for enhancing the wear (tribological) and mechanical behaviours of Al/Mg-based matrix composites [8–10]. A higher texture index was produced in the microstructure of the multiple pass FSP'ed Mg–3Al-0.2Ce alloy as compared to the tilted basal texture recorded in the single pass FSP'ed counterpart [11]. Hu et al. [12] discovered that the multiple FSP (passes) processing of the LA103Z Mg–Li alloy improved the plasticity, elongation (109%), corrosion resistance, hardness, and tensile strength of the alloy. Luo et al. [13] studied the multi-pass FSP-processed as-cast AZ61 Mg alloy and it was found that macro-defects were eliminated after multiple-tool passes. However, anisotropic tensile properties were observed in the processed alloy at elevated temperatures owing to the non-uniform texture. In another study, the low texture intensity and the high value of the Schmid factor along the processing direction were linked to the improvement in the elongation of the multi-pass FSP-processed AZ61 Mg alloy [14]. The multi-pass FSP processing of the Mg–Y-Gd-Zn-Zr alloy was also investigated by Guan et al. [15]. It was revealed that numerous original long-period-stacking-ordered (LPSO) phases became broken at the stir zones while the transformation of the LPSO phases from block to needle-like shapes was recorded at the interfacial zone owing to the short-range atomic diffusion and stacking faults. The enhancement in the ultimate tensile strength (367 MPa) and the yield strength (305 MPa) of the multiple pass FSP'ed sample was attributed to the LPSO phase and grain refinement strengthening mechanisms.

Reinforcements like B_4C [16,17], SiC [18], TiC [19–21], MWCNTs [22], nano-hydroxyapatite [23], Al_2O_3 [24] have been utilized in developing Mg matrix composites via the FSP in literature. A few studies are available on the multiple FSP processing of Mg-based hybrid composite. Recently, Yousefpour et al. [25] investigated the AZ91/HA + Ag hybrid composite developed by triple-pass FSP processing. Grain growth was suppressed due to the formation of high content of the Mg_xAg_y phase in the composite. The induced temperature coupled with the mechanical stirring effect caused the

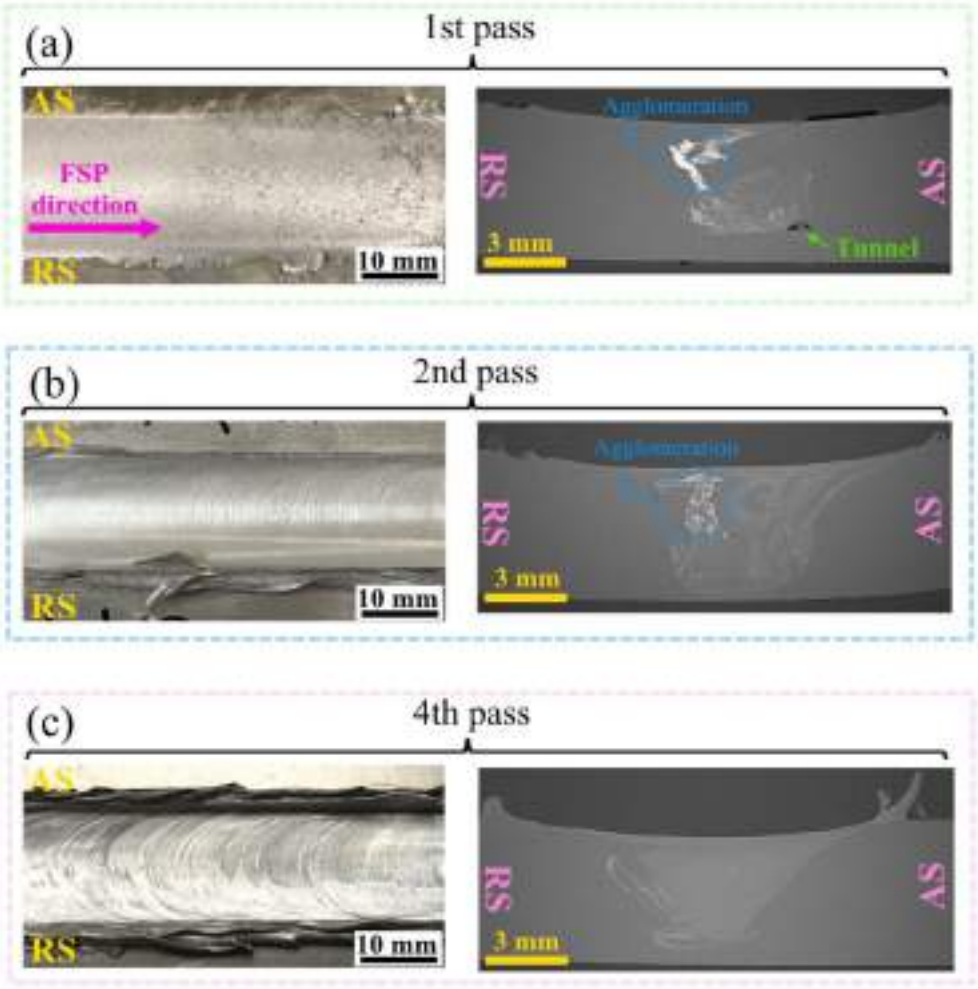

Fig. 4 – FSP processed composite after (a) first, (b) second, and (c) fourth tool passes.

dissolution of the beta phase into the alpha, and this, in turn, decreased the content of the $Mg_{17}Al_{12}$ phase in the composite. The ultimate tensile strength of the resultant composite increased to about 292 MPa while the elongation and energy absorption of the composite decreased to about 5.6% and 12.3 J/cm3 respectively. The decrease in the mechanical performances of the composite was owing to the presence of high content of Ag-rich precipitates in the composite. Eivani et al. [26] also developed the WE43 Mg/nano-sized hydroxyapatite composite via multiple FSP processing (1–6 passes). Pronounced refinement of grains and 2nd phase particles was reported to have occurred due to the repeated FSP tool passes. This attribute improved particle distributions and their fragmentation as well as the corrosion resistance of the alloy.

Based on the existing literature, the fabrication of hybridized Mg alloy/$(CeO_2+ZrO_2)_p$ composites using multiple tool pass-strategy is yet to receive significant scientific elucidation. The CeO_2 is one of the rare earth oxides with good electrochemical and thermal stabilities [27,28] while the ZrO_2 is a very stable oxide [29]. The combination of these attributes can further advance the mechanical (loadbearing), corrosion, and tribological behaviours (wear rate/mass loss, worn debris and surface) of the Mg alloy/rare-earth oxide composites. In view of this and to ensure homogeneous particle distribution, the friction stir processing of the AZ31BMg/(CeO_2+ZrO_2) hybrid composite with a multiple-tool pass strategy was investigated. The microstructure, mechanical properties (tensile and hardness), corrosion, and wear/tribological behaviours of the resulting hybridized AZ31BMg/(CeO_2+ZrO_2) composite were studied.

2. Materials and test procedures

The as-received AZ31B–Mg alloy sheets (thickness of 5 mm), and particulates of zirconium and cerium oxides (ZrO_2 and CeO_2) were applied for this experimental investigation. The base metal's properties include: ultimate tensile strength (UTS) of 241 MPa, yield strength of 153 MPa, elongation of 13%, and hardness of 72 HV. Fig. 1 displays the SE–SEM micrographs of the CeO_2 and ZrO_2 powders with mean particle sizes of 12 and 8 μm respectively.

The FSP method was utilized for developing the hybridized composites. Pre-FSP process activities were carried out before

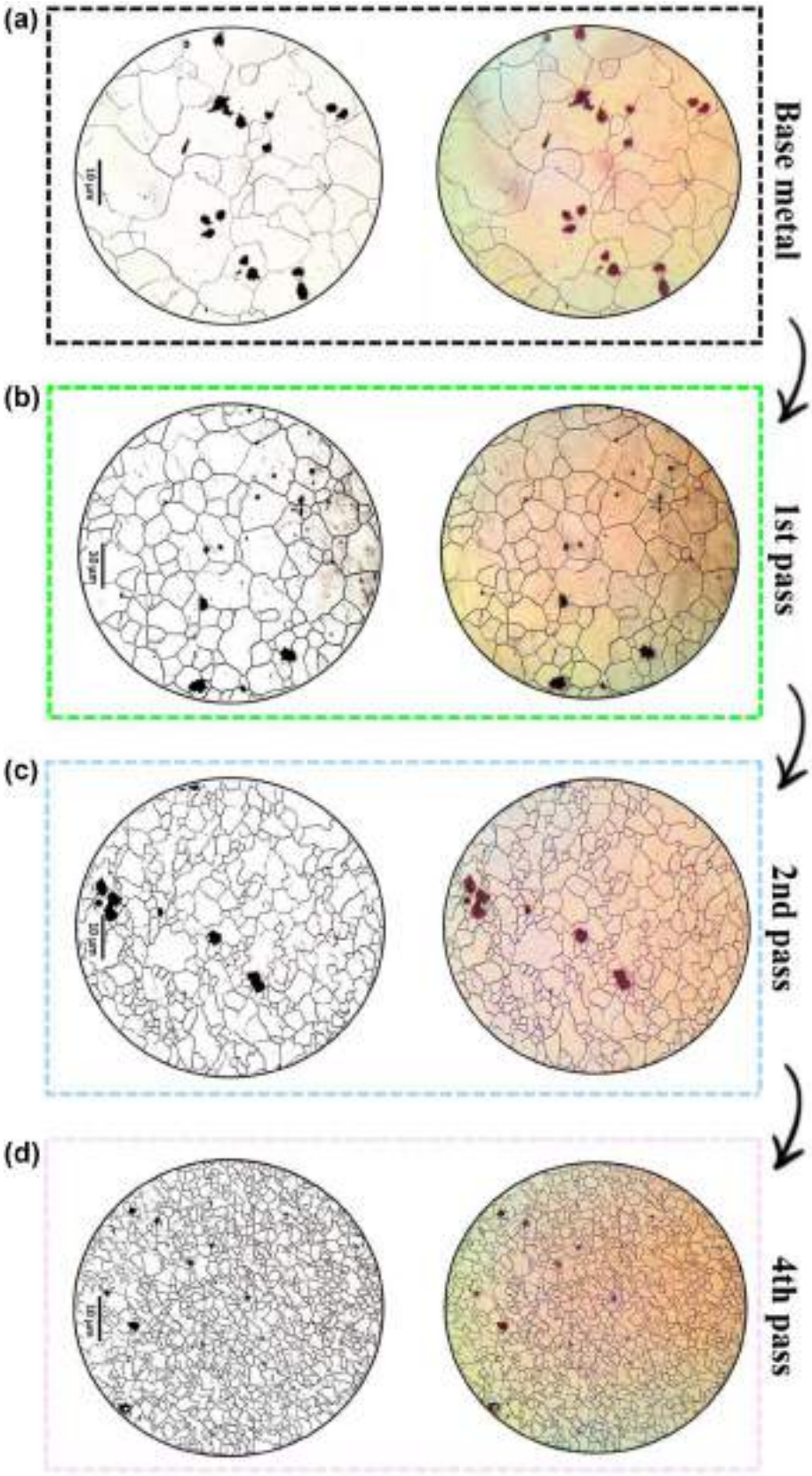

Fig. 5 – Microstructure of (a) base material; and the processed composite after (b) 1st, (c) 2nd, (d) 4th tool passes.

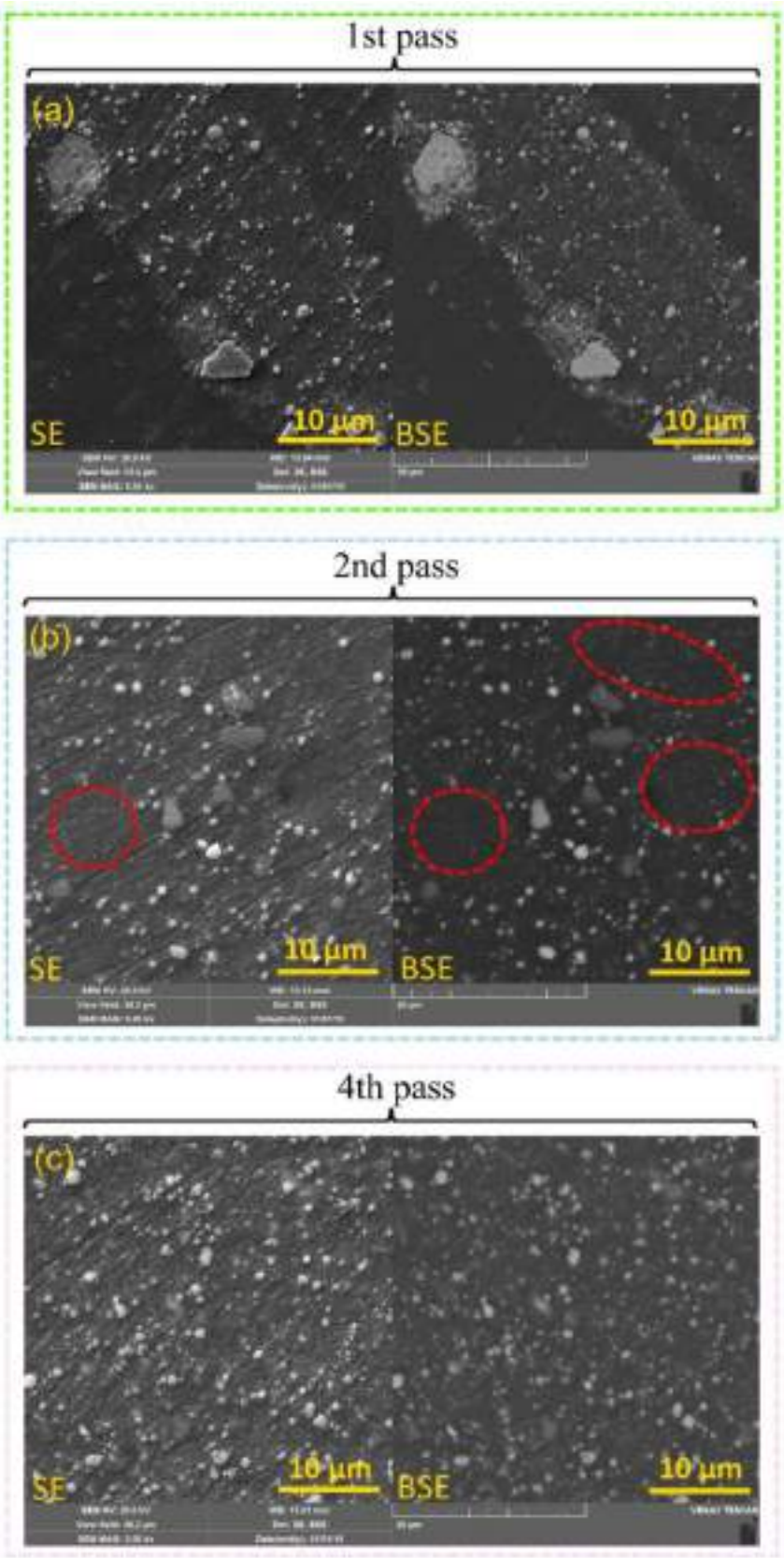

Fig. 6 – Particle distributions in the FSP processed composite after (a) first, (b) 2nd, (c) fourth tool passes.

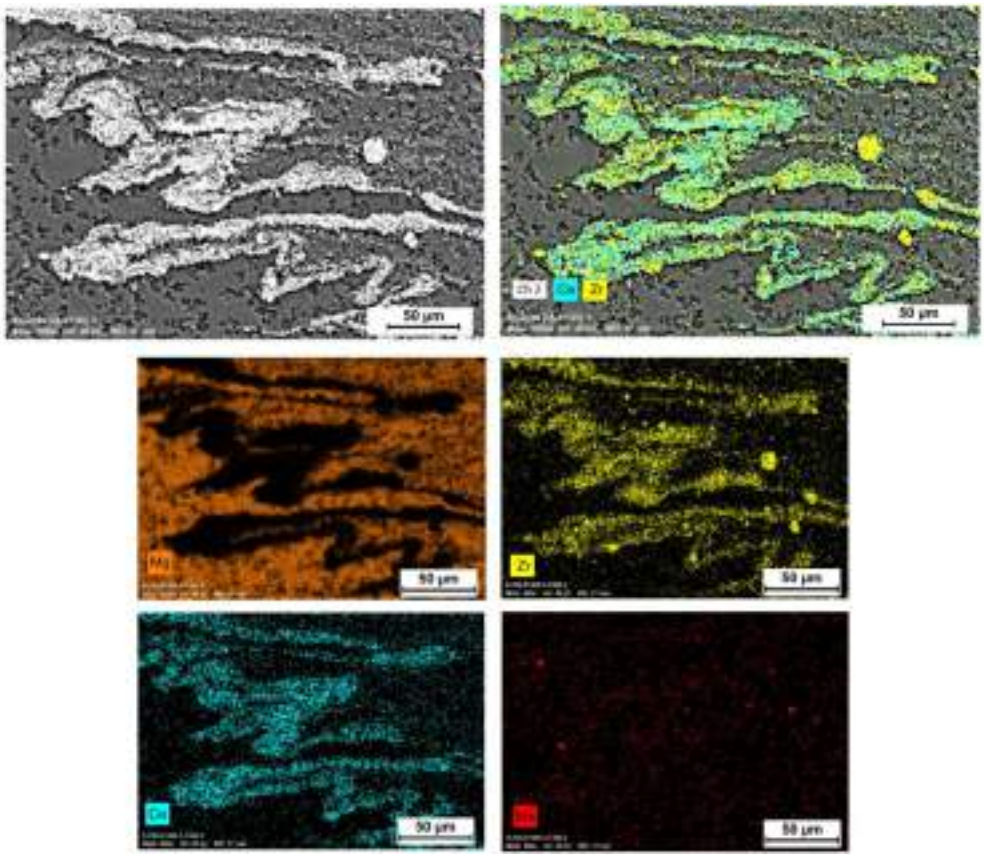

Fig. 7 – Close-up view and EDS maps of the FSP processed composite after the first (1st) tool pass.

the commencement of the actual FSP process. This involves the cutting of a rectangular groove on the base Mg alloy. The fabricated grooves have a depth of 3 mm and a width of 0.5 mm. The machined groove was filled/packed with the particulates of the rare-earth oxides (CeO_2 and ZrO_2). Then, the FSP processing commences with the preliminary process, which involves using a pin-less tool (H13 tool) to cover the surface of the filled groove via a plastic deformation mechanism as shown in Fig. 2a. The actual FSP process for the development of the composite is carried out with a probe tool as shown in Fig. 2b under multiple-tool passes. The dimensions of the tools employed for the preliminary and actual FSP processes are specified in Fig. 2. Single pass (1-P), double-pass (2-P), and 4 passes (4-P) of the FSP tool were employed for developing the hybridized composites while the other process parameters (100 mm/min and 800 rpm) were unchanged.

The processed composites were cut via the EDM wire cutting as illustrated in Fig. 3a to obtain the tensile, wear, microhardness, and microstructural samples. The cross-sectioned composites (microstructural samples) were held in epoxy-resin, and then metallographically prepared (grinding and polishing). The polished samples were etched in 100 ml ethanol +25 ml acetic acid +25 ml water +2.5g picric acid. The structures of the FSP-processed samples were examined in an OM (optical microscope), and the features that could not be found in OM were obtained using the scanning electron microscope (SEM). Further details about the structure of the composites were also investigated via transmission electron microscope. Microstructural image analysis was also carried out to acquire quantitative data such as the sizes and the distribution of grains and the embedded particles/reinforcement in the Mg alloy.

The details of the fabricated tensile specimen are specified in Fig. 3a. The tensile strengths of hybridized composite were examined following the ASTM E8M standard at an unchanged speed of 1 $mmmin^{-1}$ using a universal tensile machine (INSTRON 5500R). Also, the Vickers hardness test was conducted on the fabricated composites with a constant load (50 g) and dwell (10 s). The pin-on-disk (POD) wear type was performed on the hybrid composites as revealed in Fig. 3b and illustrated in Fig. 3c. The wear test was performed using the following parameters: 1 cm pin diameter, 40 N force, and 26.04 rpm pin speed. The wear rate (in mg/m) of the hybridized composite was estimated by dividing the wear loss (mg) with the sliding distance (m). The worn debris and surfaces of the composites were also examined in the scanning electron microscope to gain further understanding about the wear behaviour. The 3-electrode electrochemical cell test was carried out on the hybridized composites. The corrosion properties (current densities and potentials) of the different test samples were compared with the corroded surfaces. The corroded surfaces of the composites were examined in SEM.

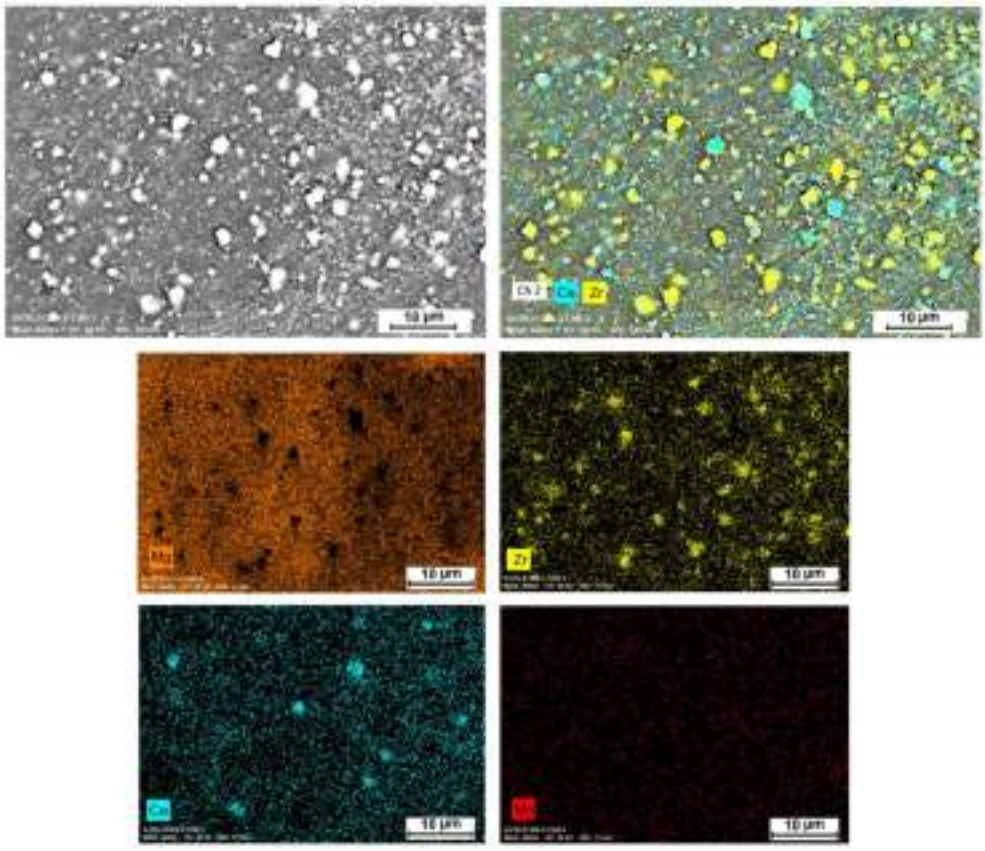

Fig. 8 – Close-up view and EDS maps of the FSP processed composite after the 4th tool pass.

3. Results and discussion

3.1. *Composite's external appearance and microstructure*

The surface morphologies and the cross-sectioned views of the hybridized composite after the tool's single and multiple passes are shown in Fig. 4. The appearances of the flash and the stirred section of the hybrid composites vary as the tool passes were raised from 1 to 4 in Fig. 4a–c. The amount and thickness of the squeezed-out flash increased in the composite samples after the rise in the tool's passes due to the improved plastic flow. The rise in the tool's pass number from 1 to 2 smoothens the surface area of the composite and a more reflective surface is accomplished after the 4th pass owing to the multiple plastic deformations and material flow. Tunnel-like defects and clusters or agglomeration of CeO_2+ZrO_2 particles are present in the cross-section provided in Fig. 4a (1st tool pass). The flow-related defect was eliminated after the 2nd passing of the tool in Fig. 4b; however, particle agglomeration could not be prevented. A further rise in the tool's pass number to four (4) prevented particle clustering/agglomeration as well as a flow-related defect in the cross-section of the composite in Fig. 4c. This observation shows that multiple-tool passes aids better plastic material flow and distribution of the particles in the Mg matrix.

The microstructures of the base alloy and the hybridized composites are provided in Fig. 5. Coarse grains are present in the as-received base Mg alloy (AZ31B). However, the refinement of the grains ensued after the FSP processing due to the dynamic recrystallization effect. Fine equiaxed grains are formed in the composite after the 4th pass of the tool. This shows that the increase in the tool's pass number did not induce grain coarsening. The existence of fine CeO_2+ZrO_2 particles in the Mg alloy is considered to have hindered the coarsening/growth of grains in the magnesium matrix even after multiple-tool passes. It is considered that the consecutive FSP tool passes lead to multiple plastic deformations and accumulative refinement of the composite. Qiao et al. [1] revealed that the entanglement of HAGBs in the ZrO_2-reinforced Mg composite aided the development of fine recrystallized grains in the hybridized composite due to the effect of the multiple-tool passes. This was indicative of the existence of continuous dynamic recrystallization during the FSP. The FSP process could be said to have created a large number of low-angle grain boundaries (LAGBs) and misoriented sub-grains, which are favored sites for nucleating recrystallization [2]. The transformation of the LAGBs to HAGBs via continuous dynamic recrystallization was acknowledged to have aided the growth of the fine nuclei to perfectly fine equiaxed grains [2]. The particulates (CeO_2 and ZrO_2) in the matrix alloy are not discernible in Fig. 5. Therefore, the microstructural samples of the composites are viewed in

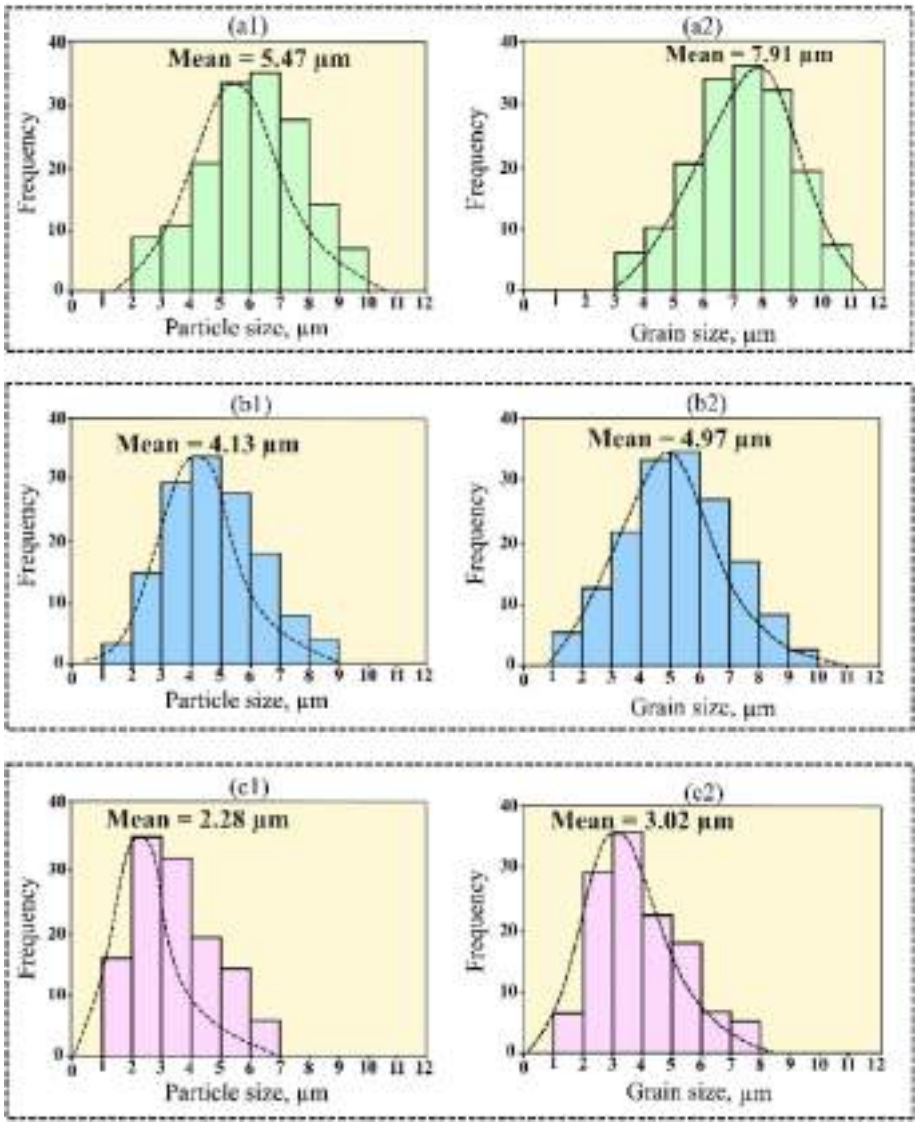

Fig. 9 – Particle and grain distributions and sizes of the FSP processed composite after different tool passes (a1) and (a2) particle and grain sizes after the 1st tool pass; (b1) and (b2) particle and grain sizes after the 2nd tool pass; (c1) and (c2) particle and grain sizes after the fourth (4th) tool pass.

the SEM to observe the inherent particles in the composites. The FE-SEM imageries of the FSP processed composites are presented in Fig. 6. The distribution level of the particles in the composite is meaningfully enhanced as the number of the FSP passes were raised. Particle-free zone and large (or clustered) particles are found in Fig. 6a owing to insufficient material flow-induced particle distribution after the first tool pass. The dispersion level of the CeO_2+ZrO_2 particles was enhanced after the second tool pass but the particle-free zone could not be entirely circumvented in Fig. 6b. The red dotted circles in Fig. 6b indicates the stirred regions having little or no $(CeO_2+ZrO_2)_p$ particles. Fig. 6c shows a uniform distribution of the reinforced particles without a palpable particle-free zone. Similarly, the level of the interparticle distance of the FSP processed composite is indirectly proportional to the level of the tool passes. Significantly close interparticle distance is observed in Fig. 6c compared to other samples in Fig. 6a and b. Qiao et al. [1] reported that the ZrO2 particles were fully mixed with the AZ31 Mg matrix after the 4th tool pass. This outcome led to uniform particle distribution without any vacancies and aggregations.

The EDS mappings of the fabricated composites after the tool's first and fourth pass numbers are shown in Figs. 7 and 8 respectively. The yellow and blue colors represent the Zr and Ce elements respectively, which are indicative of the embedded ZrO_2 and CeO_2particles respectively. Clusters of the Zr and Ce are found in Fig. 7 and this validates that significant dispersion of the CeO_2+ZrO_2 particles was not established after the 1st tool pass. On the other hand, even and finely dispersed CeO_2+ZrO_2 particles were formed after the tool's fourth pass in Fig. 8 owing to the successive number of tool passes.

The quantitative assessments of the particles as well as the average grain distributions of the hybridized composites

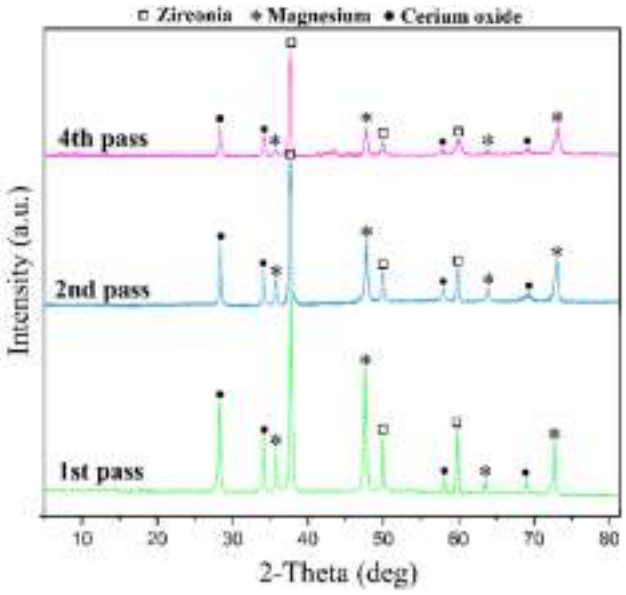

Fig. 10 – XRD of the hybridized composite after different tool passes.

were carried out and the required plots for these are given in Fig. 9. The mean sizes of the particles (rare-earth oxides) in the composite were 5.47, 4.13, and 2.28 μm after first, second, and fourth passes respectively. The average grain sizes of the hybridized composite likewise reduced from 7.91 μm (1st tool pass) to 4.97 μm (2nd tool pass), and 3.02 μm (4th tool pass). The successive severe plastic straining after increasing the tool's pass number is considered to have facilitated the disintegration/refinement of the reinforced particles in the composite. The severe straining of the reinforced particles during the succeeding tool's pass is a prominent factor for the modification of the sizes of the reinforcement particles. The fine particles then act as restraining particles that hamper the movement of grain boundaries or grain growth in the composite. As a result, Zener pinning and dynamic recrystallizations are identified as the mechanisms aiding the inhibition of grain growth in the fabricated composite after increasing the FSP passes. The fine reinforced particles in the Mg matrix facilitated finer microstructure owing to the pinning of grain boundaries and particle stimulate nucleation phenomena [2]. Dynamic recrystallization ensues in the composite due to the repeated frictional heat and the straining/mechanical stirring effects during the FSP

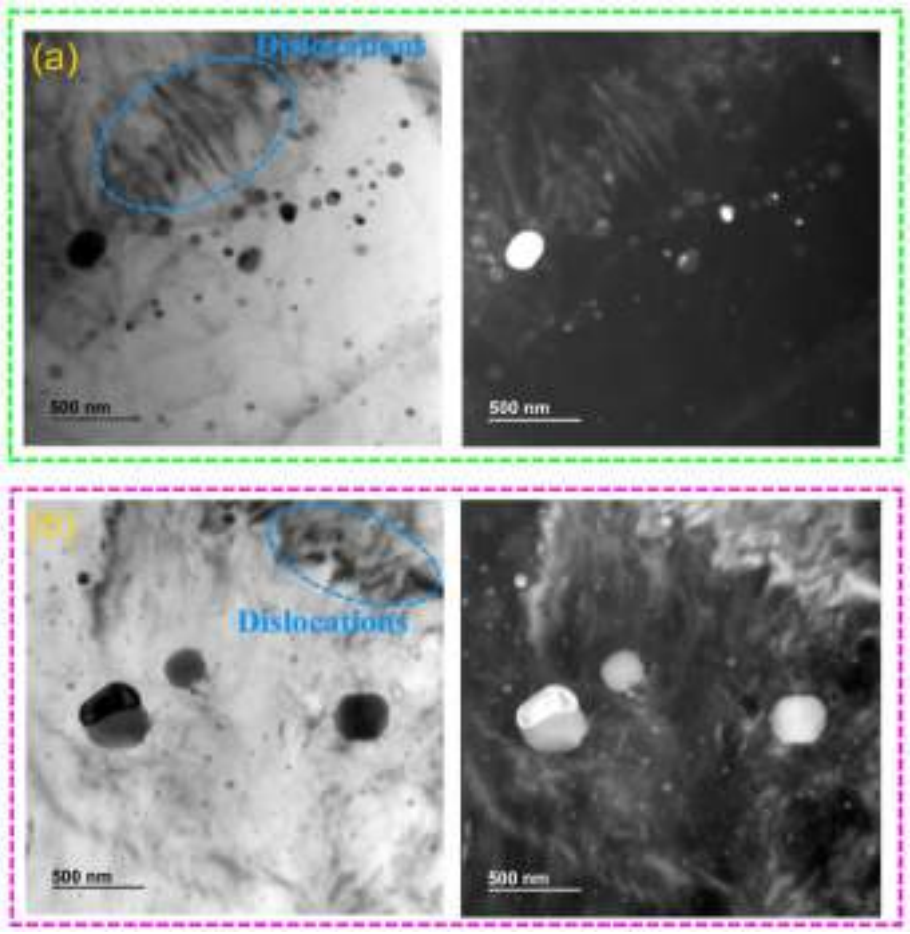

Fig. 11 – TEM imageries of the developed composite after (a) 4th, (b) 1st tool passes.

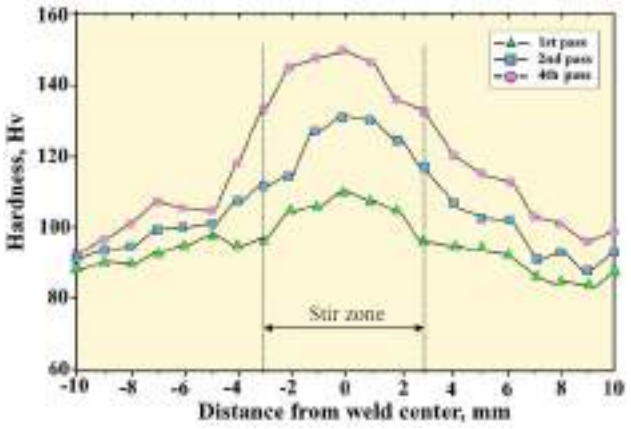

Fig. 12 – Microhardness plots of the FSP processed composite after 1–4 tool passes.

process. Subgrain particles can be formed along the grain boundaries of the hybridized composite to hinder the movement of the grain boundaries and grain coarsening after the dynamic-recrystallization action at the stirred zone [25] (see Fig. 10).

The XRD peaks reveal the existence of the Mg, and the rare earth oxides (ZrO_2, and CeO_2) as the phases in the hybridized

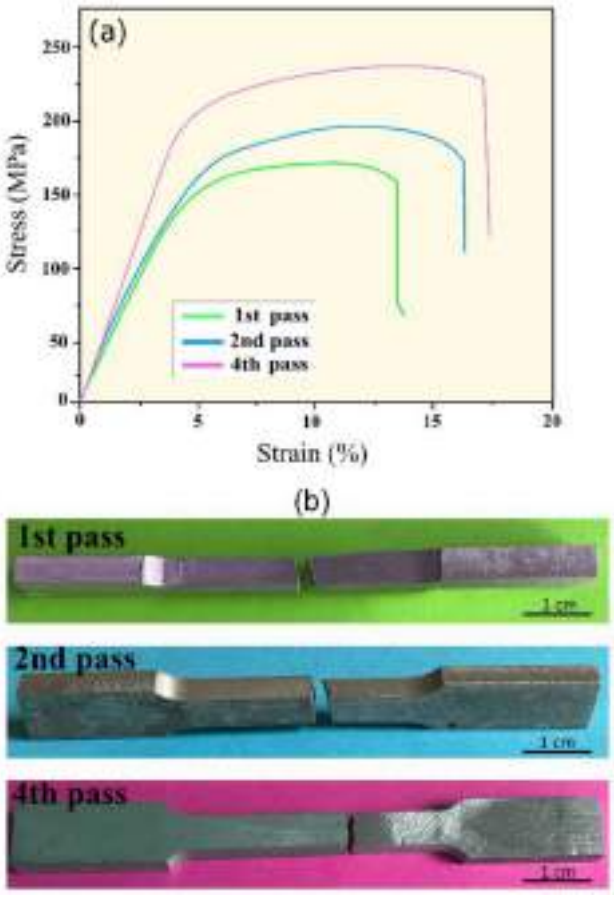

Fig. 13 – Tensile loading results of the FSP processed composite (a) stress-strain curve, (b) fracture location.

composite regardless of the tool's pass number. This shows that the increment in the FSP passes up to 4 does not cause any interaction between the reinforcement particles and the matrix. The TEM imageries of the FSP processed composite after the first (1st) and fourth (4th) tool passes are shown in Fig. 11b and a respectively. The images validate the existence of finer reinforcements/particles in the sample processed with the fourth (4-P) pass as compared to the 1st tool pass-processed composite. The regions with high dislocation density are present in both Figs. 11a and b regardless of the level of the tool passes. This could be credited to the combined impact of severe plastic deformation, sub-grains, and differential strains between the particles and matrix. The matrix-particle interface appears to be clear without any palpable gap. The appearance (discrete) of the matrix-particle interface was recognized as a testament to the nonappearance of particle-matrix diffusion [30].

3.2. *Hardness, tensile, wear and corrosion properties*

3.2.1. *Hardness*

The microhardness plots of the FSP-processed composite after single and multiple tool passes are plotted in Fig. 12. A direct relationship occurs between the tool's pass number and the hardness of the stirred centre. The hardness of 112, 133, and 151 HV were found at the centres of the samples processed with the first (1st), second (2nd), and fourth (4th) passes respectively. Generally, microhardness distribution is always affected by grain size, phase composition, and distribution. The microstructure assessment did not show any phase or compositional changes after processing the hybridized composite with different tool passes. Consequently, the mean particle and grain sizes of the developed composites could be said to have had a dominant impact on the microhardness value of the composite. The refinement of grain and particles of the AZ31B Mg/$(CeO_2+ZrO_2)_p$ hybrid composite ensues with the rise in the tool's pass number. The microhardness value of the composite is thus enhanced by grain size fine-tuning owing to the grain-refinement strengthening mechanism. Liu et al. [31] reported that the microstructural modification induced by the FSP process relatively increased the content of TiC and $Al_{12}Mg_{17}$ phases due to the structure refinement, and this aided the improvement of the microhardness values of the Al–Ti/CNTs/TiC/AZ31 composite. The hardness enhancement in the composite can be related to particle-assisted strengthening mechanisms like Hall-Petch relationship impact (grain size refinement) and Orowan strengthening (particle dispersion) [32].

3.2.2. *Tensile behaviour*

The tensile results (plots) of the FSP processed composite after varying pass-numbers of the tool are presented in Fig. 13. The tensile strengths of 172, 198, and 239 MPa were for the composites processed with the first (1st), second, and fourth (4th) tool passes respectively. This shows that the increment in the FSP pass directly improves the tensile strength of the hybridized composite. This may be connected with the elimination of flow-assisted defect and particle agglomerations in the (CeO_2+ZrO_2)-reinforced composite as the FSP pass is elevated. The clustered particles or large presence of hard

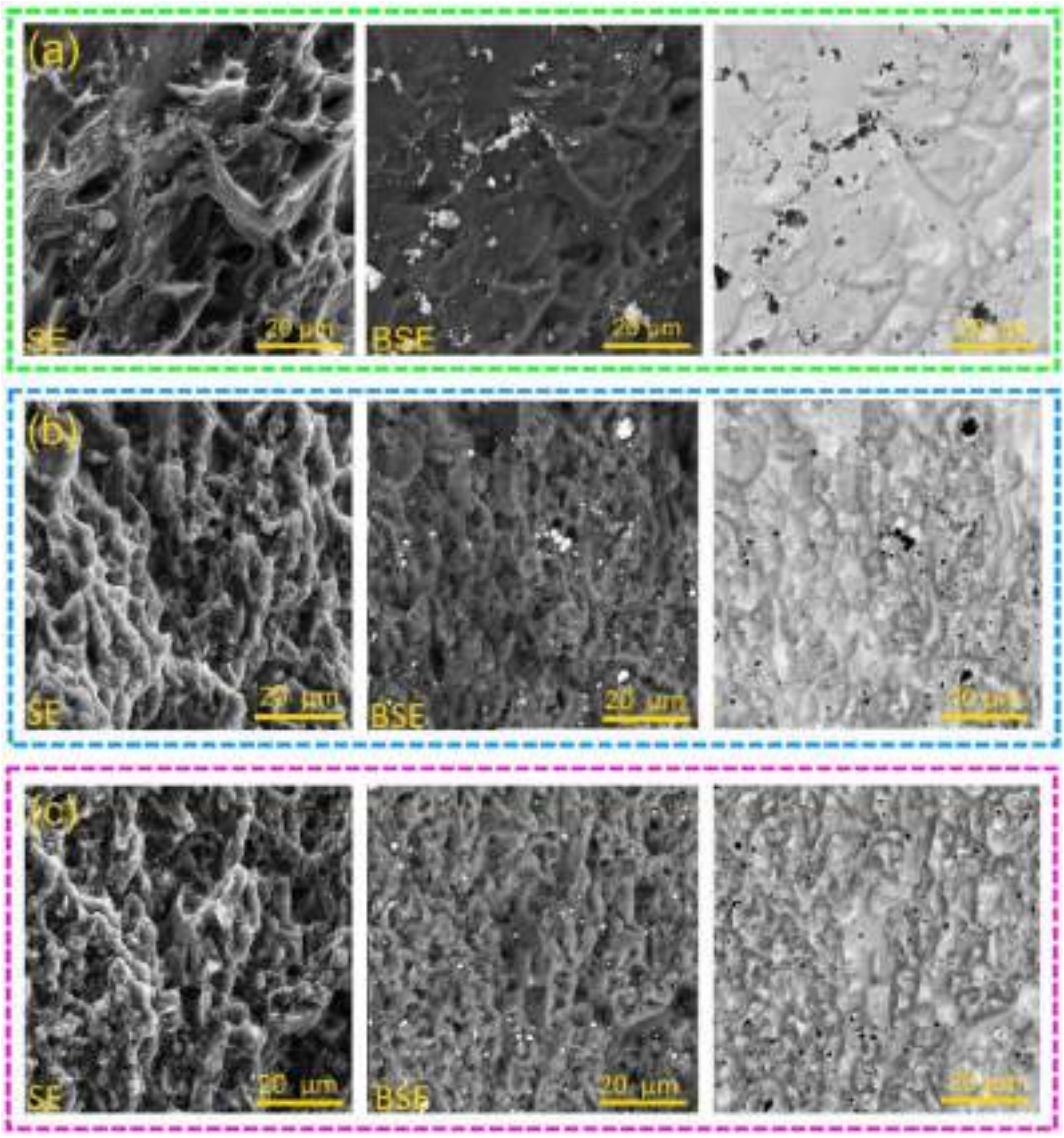

Fig. 14 – Fractures of the FSP processed composite after (a) 1st, (b) 2nd, and (c) 4th passes.

particles at the grain boundary zone (or grain interior) were reported to have induced large stress concentrations in the denser particle region [32]. This region was prone to quick crack initiation and propagation during the tensile test. This behaviour could a factor facilitating the lesser strength of the composite with the clustered CeO_2+ZrO_2 particles. The upgrade in the tensile strength of the hybridized composite as the tool's pass number is raised may be associated with the better spreading of the $(CeO_2+ZrO_2)_p$ particles and grain refinement. Many researchers have also attributed the improved tensile responses of composites to grain refinement (recrystallized grains), thermal expansion mismatch-aided strengthening, dislocation-strengthening, and particle-aided strengthening or Orowan strengthening mechanisms [32–35]. Meanwhile, the improvement in particle distribution as the tool's pass level is increased is a major factor that improved the strength of the hybridized composite. Sufficient material/plastic flow, particle dispersion with tangles of dislocation and even the presence of finer grains in the matrix were reported as the factor aiding the improved ultimate tensile strength of the composite [36].

The fracture surfaces of the FSP-processed composite after varying passes of the tool are revealed in Fig. 14. The SE and BSE-SEM images of the composites show uneven fracture surfaces characterized by the presence of shallow dimples. The number of dimples in the BSE-SEM image provided in Fig. 14a is lesser than that of Fig. 14b and b. This is indicative of a lesser loadbearing attribute in the 1st pass-processed composite and this observed finding validates the tensile results provided in Fig. 13. However, the difference between Figs. 14b and c could not be ascertained due to the similar fractographic properties such as shallow dimples across the entire fractured surface of the composite. It can thus be concluded that the developed composite exhibits ductile fracture behaviour regardless of the tool's pass level. The EDS mapping of the fractured surface of the 4th pass-composite is given in Fig. 15

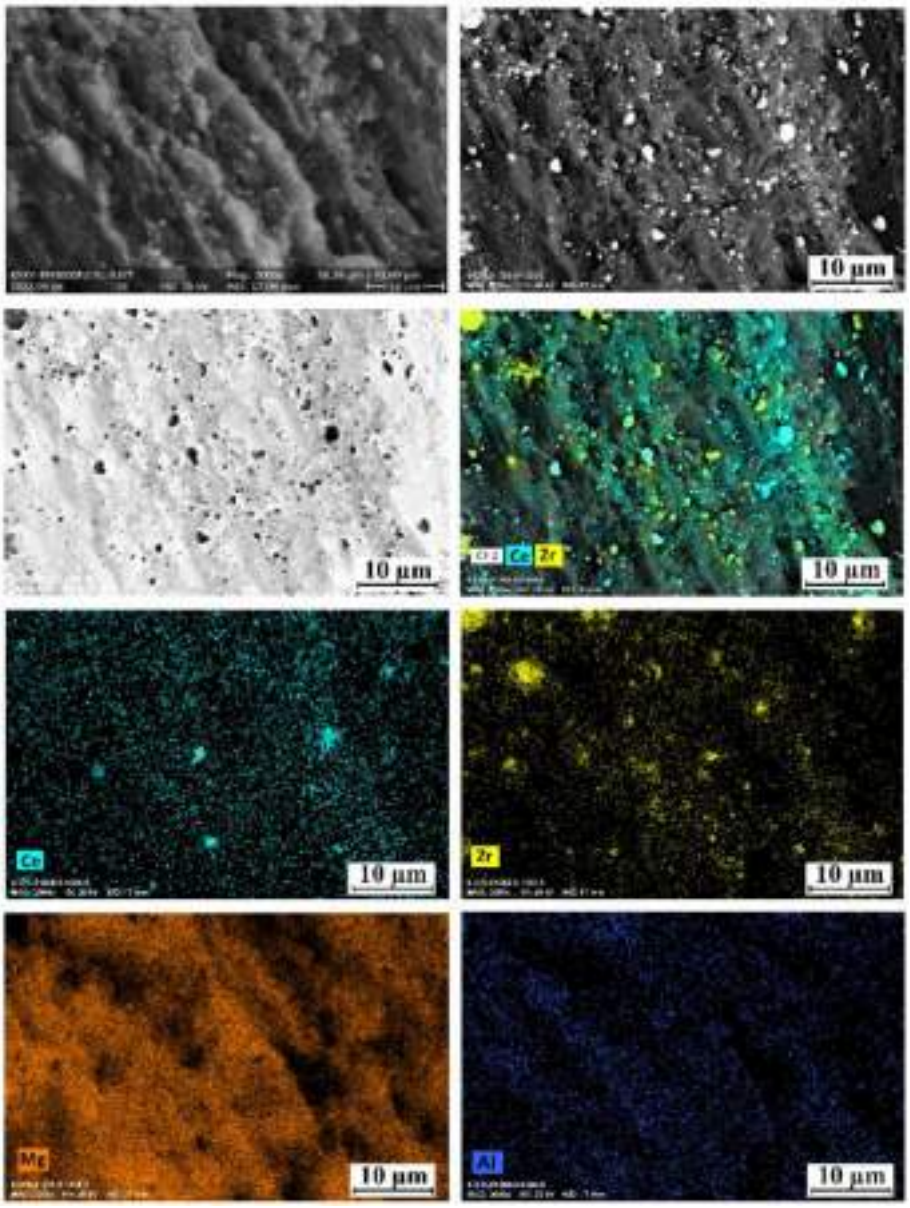

Fig. 15 – MAP of the FSP processed composite after fourth pass.

while the XRD of the fracture samples are shown in Fig. 16. The $CeO_2$and ZrO_2 particles are present on the fracture surfaces of the composite. The existence of fine reinforced particles across the fractured surfaces of the composite in Fig. 15 is a testament to the occurrence of particle-induced strengthening mechanism in the composite. Dinaharan et al. [37] acknowledged that the existence of Ti particles across the fractured surfaces of the AZ31/Ti composites was an indication of superior particle-matrix interfacial bonding.

3.2.3. *Wear properties*

Fig. 17 provides the wear properties of the hybridized composite after the different number of tool passes. The mass loss-sliding distance plots of the developed composites after the wear test is provided in Fig. 17a. A steady-state wear regime is achieved after the initial running-in regime as indicated in Fig. 17a. A direct interrelationship is observed to exist between the mass loss (g) and the distance (m) in Fig. 17a. However, the amount of mass loss declines with the rise in the tool's pass level. On the other hand, the wear rate (mg/m) of the composite significantly decreased after the increment in the pass number. The specific-wear rate of the composite (see Table 1) also decreased from 4.26×10^{-5} to 2.17×10^{-5} mm^3/Nm as the pass number rose from 1 to 4. This is majorly due to the finer grains and enhanced hardness values.

Based on the outcomes of the hardness (see Fig. 12) and the wear rate (see Fig. 17a), it can be said that a direct/linear interrelationship exists between the microhardness and the rate of wear of the hybridized composite. This shows a good pact with the Archard's equation. The improvement in the dispersal of the reinforced particles coupled with the extremely close interparticle distance as the FSP pass level is

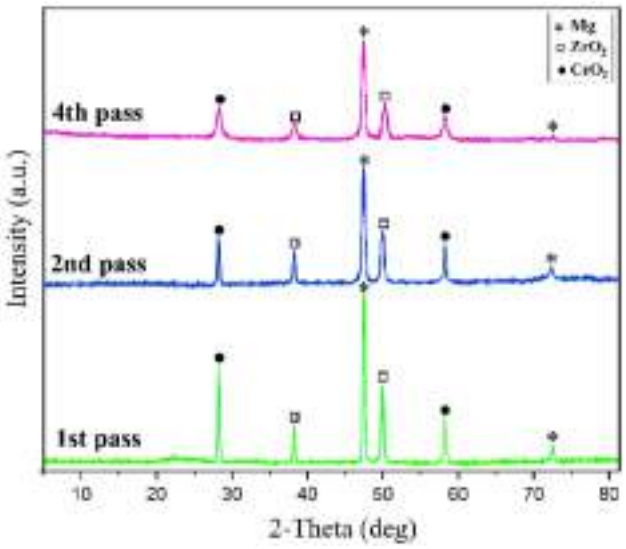

Fig. 16 – XRDs of the failed hybrid composite.

raised is reckoned as the factors aiding better wear properties i.e., mass/wear loss, and wear rate/specific wear rate. The fine and suitably spread reinforced particles in the matrix alloy could be considered to have countered immediate deformation/material loss during the wear test in the 4-P composite (4th pass) while the presence of regions with a lesser number of embedded reinforcements (CeO_2+ZrO_2) favored easy deformation, mass loss as well as wear rate in the 1-P composite (1st pass). The properly dispersed CeO_2 particle could improve the self-lubricating properties of the composite during the wear test.

The post-wear examination of the FSP-processed composite was performed to understand the wear behaviour of the composites fabricated with varying passes of the tool. Fig. 18 shows the worn surfaces of the hybridized composites. A modification in level of the FSP passes is observed to have been a major determinant in the wear behaviour of the composites due to the disparity in the worn surfaces. Delaminated areas (delamination) on the worn composite's surfaces are marked with blue dotted lines or enclosures on the SE–SEM images displayed in Fig. 18. Meanwhile, the worn surface area with delamination is quite large in Fig. 18a (1st pass-processed sample) as compared to Fig. 18b (2nd pass-processed sample) and Fig. 18c (4th pass-processed sample) respectively. This is due to the level of dispersion of the reinforced particles in the base Mg alloy. The insufficient dispersion of the particles led to the presence of a particle-free region in the 1st pass-sample. This zone devoid of reinforcement is said to have offered lower resistance to wear loss/wear rate and consequently led to the emergence of delamination in Fig. 18a while the region with clustered CeO_2+ZrO_2 particles shows smooth outlook, which is indicative of abrasive wear behaviour in Fig. 18a. The delaminated region of the hybridized composite decreased as the pass level rose from 1 to 4. As a result, a more abrasive wear mode is said to have occurred in the composite as the FSP pass level is raised because of the better material (plastic) flow and dispersion of the reinforced particles.

Fig. 19 reveals the debris of the hybridized composites after the wear test. The size of the worn debris in Fig. 19a is the largest, and comparatively, the sizes of the worn debris decline as the FSP pass level is raised to 2 and 4 respectively.

A similar trend ensues between the amount of mass/wear loss (g) and the size of the worn debris after the wear test. The increase in the wear rate or mass loss leads to an equivalent increase in the average size of the worn debris. The fine and suitably distributed particles in the Mg alloy are believed to have prevented direct contacts between the pin with the Mg matrix during testing for the wear behaviour of the composite. This attribute limits the wear rate, the mass loss, and the morphology of the worn debris as revealed in Fig. 19. The loss of particle-strengthening effect, significant matrix deformation, and tribolayer instability are recognized as the factors that aid the upsurge in the volume of worn debris during the wear test of composite [38]. In this case, the contacts of the pin with the insufficient reinforced section within the hybridized composite is adjudged to have caused significant matrix deformation and wear in Fig. 19a relative to Figs. 19b and c respectively.

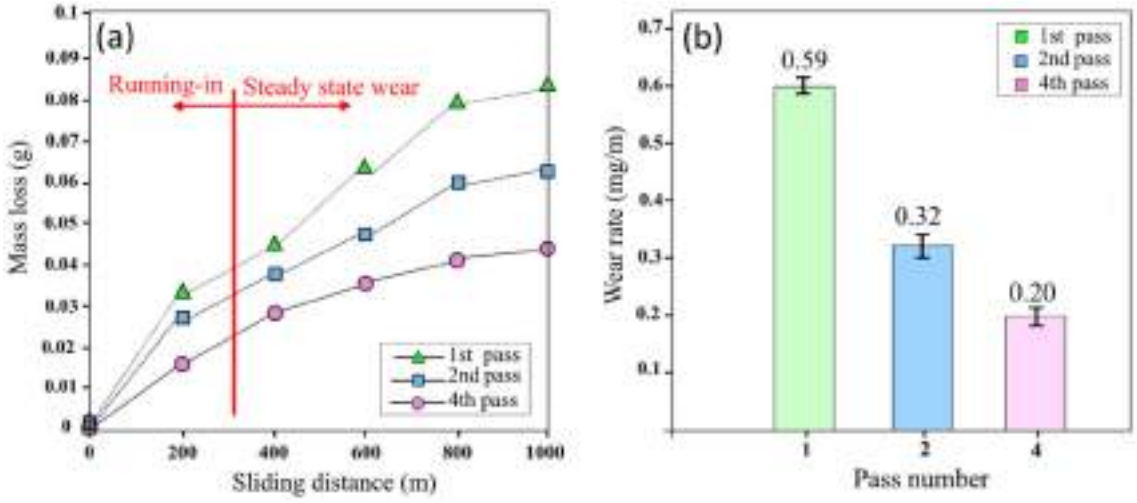

Fig. 17 – Wear of the FSP processed composite (a) mass loss against sliding distance, (b) wear rate vs. pass number.

Table 1 – Wear rate results.

Sample	Specific wear rate (mm^3/Nm)
1st pass	4.26×10^{-5}
2nd pass	3.45×10^{-5}
4th pass	2.17×10^{-5}

Fig. 20 provides the friction coefficient versus the sliding-distance of the hybridized composites. The average friction coefficient of the composites decreased from 0.45, 0.23, and 0.18 as the pass number of the tool was raised from 1 to 2 and 4 respectively. This behaviour is linked to the inherent characteristics (dispersion and finest) of the particles in the matrix of the composite. The sample with comparatively larger grains and particle size with uneven particle distribution recorded the friction coefficient in Fig. 20a. As the particle dispersion is improved, the friction coefficient of the composite declined in Fig. 20b and further reduced in Fig. 20c owing to the even particle distribution, and the reduced particle size and interparticle distance. The finely distributed $(CeO_2+ZrO_2)_p$ particles are believed to have acted as deformation-bearing obstacles during the test to enhance the wear and the friction coefficient of the composite. Amra et al. [39] reported that the formation of a stable tribolayer and solid

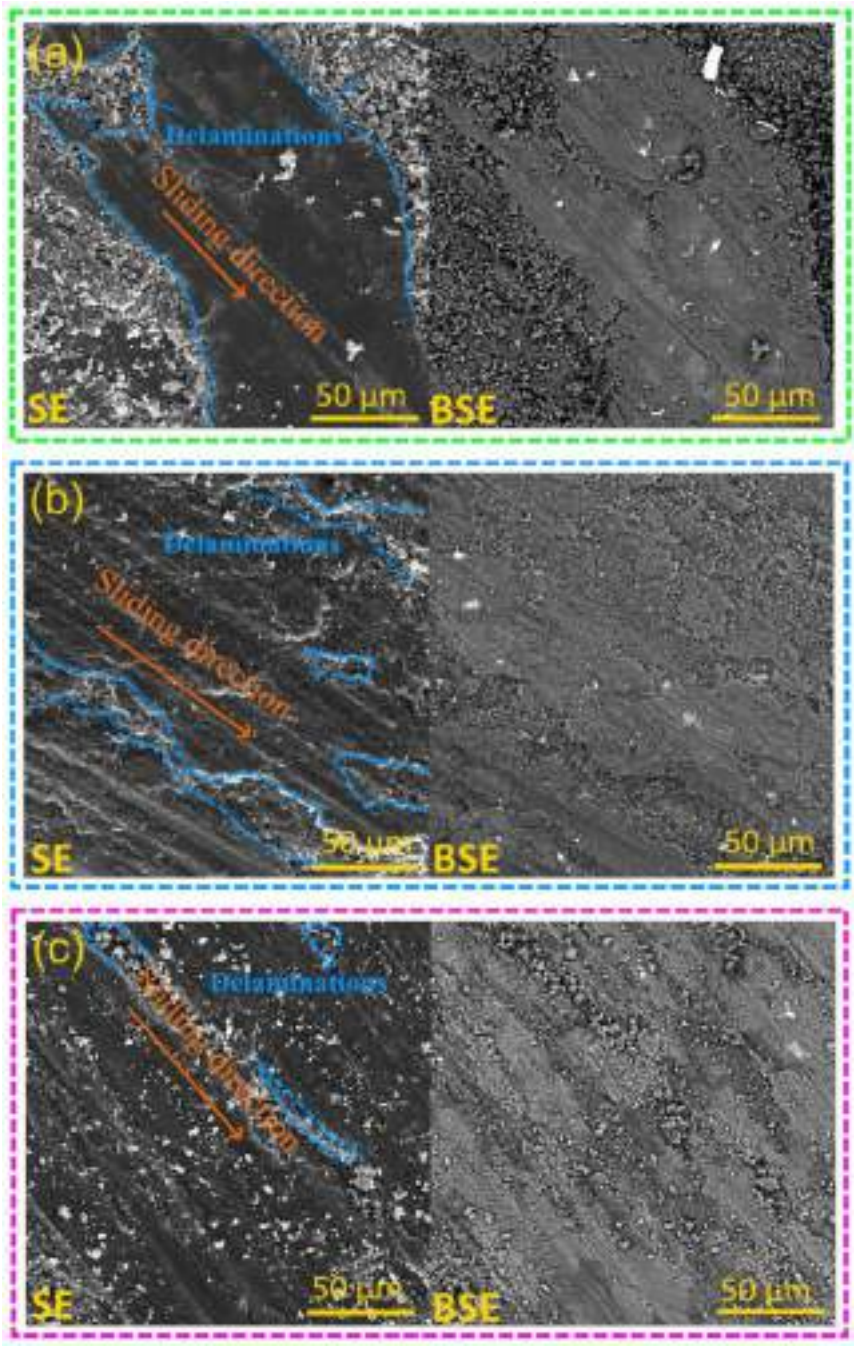

Fig. 18 – Worn areas of the FSP processed composite at (a) first, (b) 2nd, and (c) fourth passes.

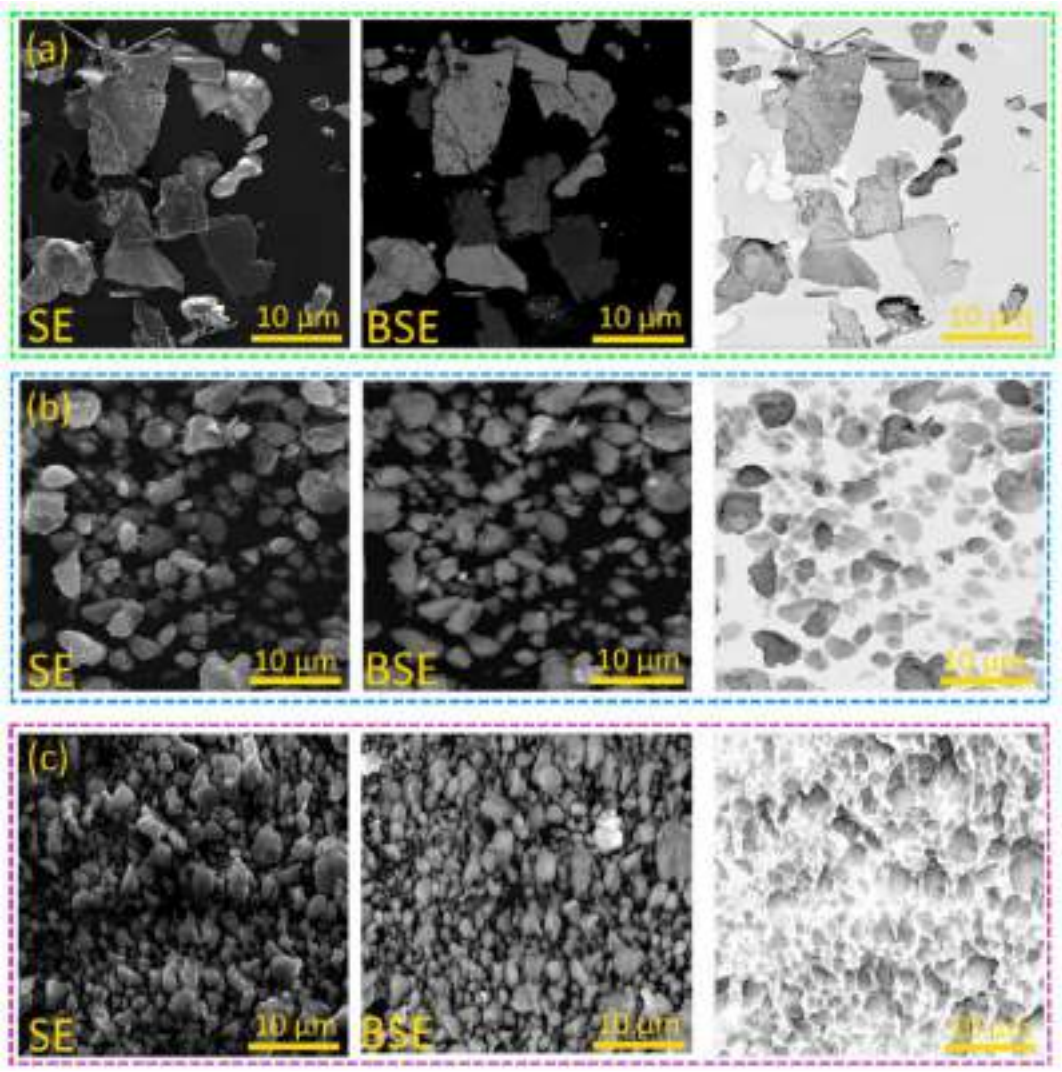

Fig. 19 – Debris of worn composites at (a) first, (b) 2nd, and (c) fourth passes.

lubricating effects as the factors that improved the friction coefficient of the friction stir processed Al5083/CeO_2/SiC composite. The self-lubricating attributes of the CeO_2 particles could have also impacted the lessening in the friction coefficient of the hybridized composite as the particle-dispersion was enhanced multiple (four) passes of the tool.

3.2.4. *Corrosion resistance*

The open circuit potentials (OCP) and the polarization plots of the FSP-processed composite are provided in Fig. 21a and b respectively. The highest OCP is obtained in the 4th tool pass-processed composite, followed by the 2nd and the 1st tool passes respectively. The corrosion properties of the hybridized composite are extrapolated and provided in Table 2. The corrosion potentials (Ecorr) of the first (1st), second (2nd), and fourth (4th) tool pass-processed composites were - 1.81 ± 0.02, −1.75 ± 0.02, and −1.64 ± 0.02 V respectively whereas their respective current densities (icorr) were 5.217 ×10^{-3}, 4.351 ×10^{-3}, and 3.074 ×10^{-3} A/cm^2. It is clear that the self-corrosion potential (~−1.64 V) of the 4th tool pass-processed composite is the highest while it has the smallest current density (3.074 ×10^{-3} A/cm^2), followed by the 2nd and the 1st tool pass-processed composites respectively. This implies that the best corrosion resistance is observed in the hybridized composite processed with 4 number of tool passes. The formation of finer particles in the Mg alloy could be responsible for enhancing the corrosion resistance of the hybridized composite. It was reported in the works of Liu et al. [31] that the resistance to corrosion attack in the Al/TIC composite improved owing to a large number of TiC and network-like $Al_{12}Mg_{17}$ phases. Surface formation characteristics and inherent phase compositions are major factors that influence the corrosion of the FSP-processed composite layers [31]. In this study, the microstructural changes in terms of grain size, particle distribution, and sizes appear to have played the dominant role in the corrosion behaviour of the hybridized composite. The samples with the smallest mean grain size and $(CeO_2+ZrO_2)_p$ particle sizes and dispersion exhibited the best corrosion resistance based on the corrosion current density and corrosion potential. The CeO_2 particles were

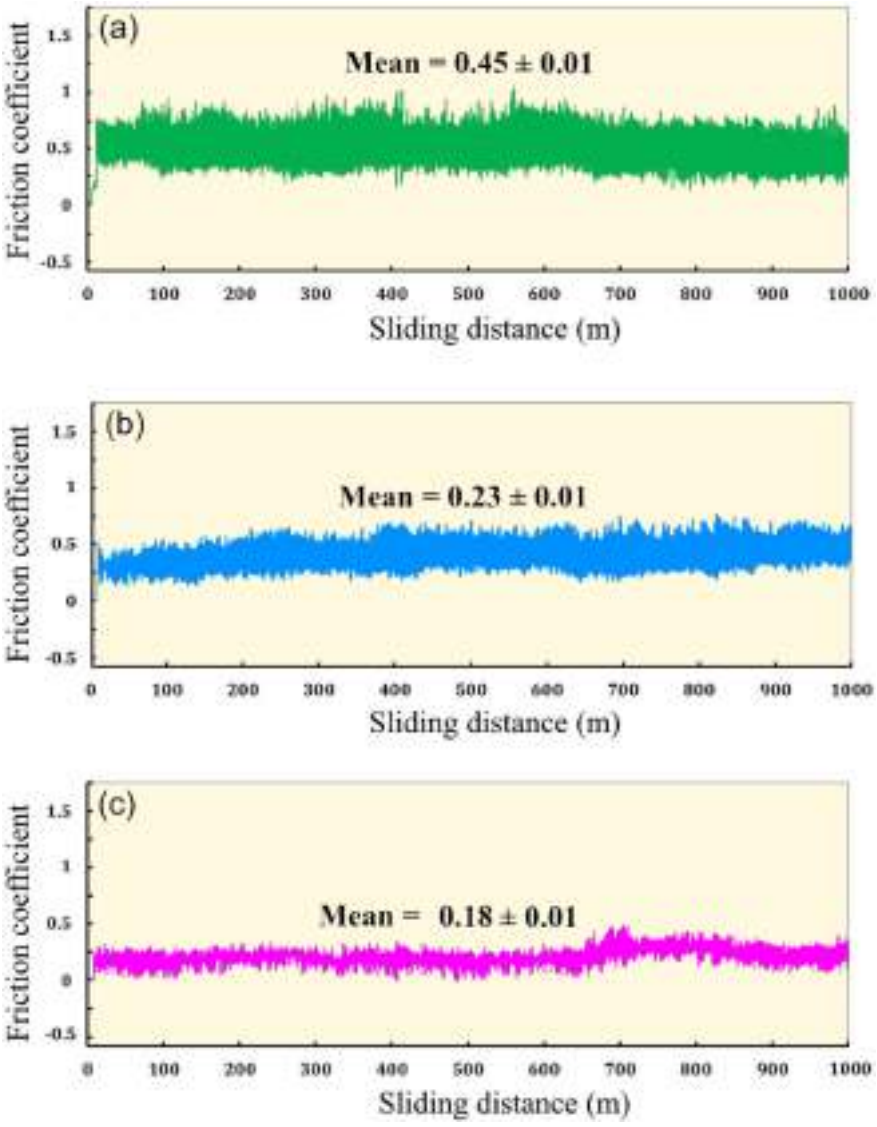

Fig. 20 – Friction coefficient against sliding distance of the FSP processed composite at (a) 1st, (b) 2nd, and (c) fourth passes.

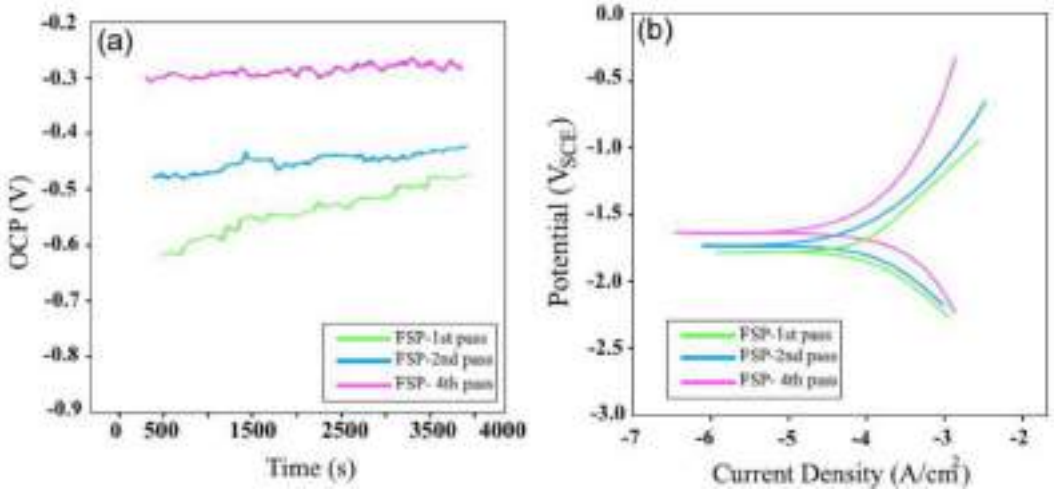

Fig. 21 – Corrosion of the FSP processed composite (a) open circuit potential, (b) potentiodynamic curves.

Table 2 – Extrapolated corrosion current densities and potentials.

Pass number	E_{corr} (V)	i_{corr} (A/cm^2)
1st	- 1.81 ± 0.02	5.217 ×10 $^{-3}$
2nd	−1.75 ± 0.02	4.351×10 $^{-3}$
4th	−1.64 ± 0.02	3.074 ×10 $^{-3}$

acknowledged to have hindered corrosion propagation in the AA7075/CeO_2/MoS_2 hybrid composite [40]. However, the finest dispersion level of the reinforced particle had a more direct influence on the corrosion resistance of the composites [41]. Thus, the direct correlation between the FSP pass level and the particle finest/dispersion is credited for the enhanced corrosion resistance of the hybridized composite.

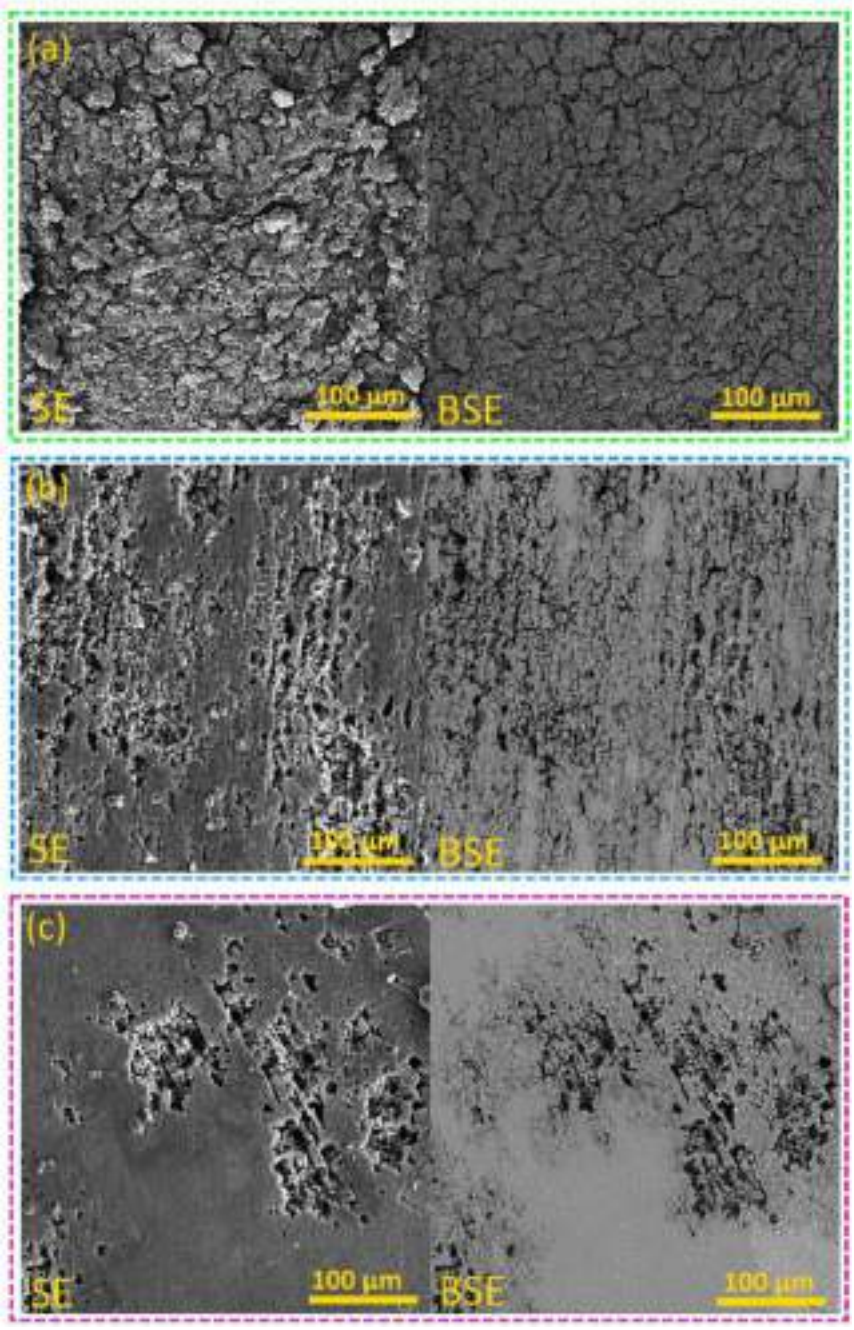

Fig. 22 – Corroded regions of the FSP processed composite after (a) 1st, (b) 2nd, and (c) 4th passes.

i The multiple-tool passes (from 1 to 4) caused the refinement of grains (7.91–3.02 μm) and particle size reduction (5.47–2.28 μm) because of the successive severe plastic straining/dynamic recrystallization mechanism, and Zener pinning effect.

ii. The rise in the tool passes from 1 to 4 did not cause any interaction between the reinforced particles and the matrix alloy

iii. The multiple-tool passes (from 1 to 4) improved the hardness values of the hybridized composite from 112 to 151 HV due to grain refinement and better particle dispersion.
iv. The tensile strength of the fabricated composite improved from 172 to 239 MPa as the pass level of the tool was elevated (1–4) owing to fine particle-aided strengthening mechanism and the elimination of flow defect and agglomeration of particles.
v. The specific wear rate and the mean friction coefficient of the hybridized composite decreased from 4.26×10^{-5}–2.17×10^{-5} mm^3/Nm and 0.45–0.18 correspondingly due to hardness improvement and CeO_2+ZrO_2 particle homogenization
vi. The corrosion resistance of the hybridized composite improved as the FSP pass level was improved from 1 to 4 by reason of grain refinement and homogeneous distribution of reinforced particles. The corrosion potentials increased from -1.81 ± 0.02 to −1.64 ± 0.02 V whereas the current density decreased from 5.118 ×10^{-3} - 3.217 ×10^{-3} A/cm^2 as the pass number was raised.

The corroded areas of the hybridized composite samples were viewed in SEM and the obtained SEM images of the samples are provided in Fig. 22. It is seen that corrosion attack could not be mitigated in the samples after varying the FSP pass level. However, the severity of the corrosion attack diminishes as the FSP pass level is raised. The entire surface area shown in Fig. 22a underwent an extreme corrosion attack with palpable corrosion pits. This form of corrosion damage could be said to have propagated along the boundaries of the grains. The presence of flow-related defect (tunnel), and insufficient spreading of the reinforced particles in the matrix might be a chief reason for such an intense corrosion attack on the hybridized composite. It was stated in the works of Zhang et al. [42] that the inherent micropores in the reinforced composite caused a significant acceleration of corrosion attack by assisting the Cl-diffusion in the matrix of the composite. The area with corrosion damage significantly decreased after the rise in the tool's pass level to 2nd (see Fig. 22b) and 4th (see Fig. 22c) respectively. This shows that the corrosion resistance is boosted as the FSP pass number is increased. It is well-reported that the corrosion current density is directly related to the corrosion rate of a test sample [31]. In this study, the highest corrosion current density implies that the corrosion rate will be intense in the 1st tool pass-processed composite as compared to the 2nd and 4th tool pass-processed composites respectively. By reducing the corrosion rate (current density), desirable or better corrosion resistance is attained as observed in Fig. 22c. The increase in pass level of the tool mitigated the corrosion damage or failure of the composite sample due to better grain refinement, and fine and homogeneous distribution of the particles [43,44]. It was reported that an indirect relationship exists between the formation rate of the protective layer ($Mg(OH)_2$) and the grain size in the studies of Qiao et al. [1]. The growth of this layer is enhanced by the presence of nucleation sites linked to grain boundary defects. As a result, the finer grain size of the composite could be said to have aided the formation of a protective layer, and this layer, in turn, acted as a barrier to ions from the NaCl solution to improve the composite's corrosion resistance.

4. Conclusions

The friction stir processing with a multiple-tool pass strategy has been employed in fabricating the hybridized AZ31BMg/(CeO_2+ZrO_2) composites. The microstructure, tensile, hardness, wear, and corrosion responses of the composites were investigated. The major findings from this study include.

Data availability' statement

No datasets were generated or analyzed during the current study.

Declaration of competing interest

The authors declare that they have no known competing financial interests or personal relationships that could have appeared to influence the work reported in this paper.

REFERENCES

[1] Qiao Ke, Zhang Ting, Wang Kuaishe, Yuan Shengnan, Wang Liqiang, Chen Shanyong, et al. Effect of multi-pass friction stir processing on the microstructure evolution and corrosion behavior of ZrO2/AZ31 magnesium matrix composite. J Mater Res Technol 2022;18:1166–79.
[2] Ahmadkhaniha D, Fedel M, Heydarzadeh Sohi M, Zarei Hanzaki A, Deflorian F. Corrosion behavior of magnesium and magnesium–hydroxyapatite composite fabricated by friction stir processing in Dulbecco's phosphate buffered saline. Corrosion Sci 2016;104:319–29.
[3] Arab SM, Akbarzadeh A. The effect of equal channel angular pressing process on the microstructure of AZ31 Mg alloy strip shaped specimens. J Magnesium Alloys 2013;1:145–9.
[4] Wang Wenke, Zhang Wencong, Chen Wenzhen, Yang Jianlei, Zhang Lixin, Wang Erde. Homogeneity improvement of friction stir welded ZK61 alloy sheets in microstructure and mechanical properties by multi-pass lowered-temperature rolling. Mater Sci Eng, A 2017;703:17–26.
[5] Zhang B, Yang C, Sun Y, Li X, Liu F. The microstructure, mechanical properties and tensile deformation mechanism of rolled AlN/AZ91 composite sheets. Mater Sci Eng, A 2019;763:138118.
[6] Orozco-Caballero Alberto, Alvarez-Leal Marta, Ruano Oscar A, Carreno Fernando. Improving the mechanical properties of a WE54 magnesium alloy through severe friction stir processing and rapid cooling. Mater Sci Eng, A 2022;856:143963.
[7] Luo XC, Kang LM, Liu HL, Li ZJ, Liu YF, Zhang DT, et al. Enhancing mechanical properties of AZ61 magnesium alloy

via friction stir processing: effect of processing parameters. Mater Sci Eng, A 2020;797:139945.
[8] Nouri Z, Taghiabadi R. Tribological properties improvement of conventionally-cast Al–8.5Fe–1.3V–1.7Si alloy by multi-pass friction stir processing. Trans Nonferrous Metals Soc China 2021;31:1262–75.
[9] Zhou Mengran, Zeng Zhuoran, Cheng Chun, Morisada Yoshiaki, Shi Qingyu, Wang Jian-Yih, Fujii Hidetoshi. Effect of the processing route on the microstructure and mechanical behavior of superlight Mg-9Li-1Zn alloy via friction stir processing. J Magnesium Alloys 2022;10:3064–81.
[10] Eivani AR, Mehdizade M, Chabok S, Zhou J. Applying multi-pass friction stir processing to refine the microstructure and enhance the strength, ductility and corrosion resistance of WE43 magnesium alloy. J Mater Res Technol 2021;12:1946–57.
[11] Gotawala Nikhil, Kumar Abhishek, Mishra Sushil, Shrivastava Amber. Microstructure and texture evolution of complete Mg-3Al-0.2Ce alloy blanks upon multi-pass friction stir processing with spiral strategy. Mater Today Commun 2021;26:101850.
[12] Hu Kai, Guan Yanjin, Zhai Jiqiang, Li Yi, Chen Fengjiao, Liu Ya, et al. Effect on microstructure and properties of LA103Z Mg-Li alloy plate by multi-pass friction stir processing. J Mater Res Technol 2022;20:3985–94.
[13] Luo XC, Zhang DT, Zhang WW, Qiu C, Chen DL. Tensile properties of AZ61 magnesium alloy produced by multi-pass friction stir processing: effect of sample orientation. Mater Sci Eng, A 2018;725:398–405.
[14] Luo XC, Zhang DT, Cao GH, Qiu C, Chen DL. High-temperature tensile behavior of AZ61 magnesium plate prepared by multi-pass friction stir processing. Mater Sci Eng, A 2019;759:234–40.
[15] Guan Xiaohu, Wang Wen, Zhang Ting, Peng Pai, Liu Qiang, Han Peng, et al. A new insight into LPSO phase transformation and mechanical properties uniformity of large-scale Mg-Gd-Y-Zn-Zr alloy prepared by multi-pass friction stir processing. J Magnesium Alloys 2022.
[16] Vedabouriswaran G, Aravindan S. Development and characterization studies on magnesium alloy (RZ5) surface metal matrix composites through friction stir processing. J Magnesium Alloys 2018;6:145–63.
[17] Paidar Moslem, Bokov Dmitry, Mehrez Sadok, Ojo Olatunji Oladimeji, Ramalingam Vaira Vignesh, Memon Shabbir. Improvement of mechanical and wear behavior by the development of a new tool for the friction stir processing of Mg/B4C composite. Surf Coating Technol 2021;426:127797.
[18] Morisada Y, Fujii H, Nagaoka T, Fukusumi M. Effect of friction stir processing with SiC particles on microstructure and hardness of AZ31. Mater Sci Eng, A 2006;433:50–4.
[19] Gobara M, Shamekh M, Akid R. Improving the corrosion resistance of AZ91D magnesium alloy through reinforcement with titanium carbides and borides. J Magnesium Alloys 2015;39:112–20.
[20] Navazani M, Dehghani K. Investigation of microstructure and hardness of Mg/TiC surface composite fabricated by friction stir processing (FSP). Proc Mater Sci 2015;11:509–14.
[21] Balakrishnan M, Dinaharan I, Palanivel R, Sivaprakasam R. Synthesize of AZ31/TiC magnesium matrix composites using friction stir processing. J Magnesium Alloys 2015;3:76–8.
[22] Morisada Y, Fujii H, Nagaoka T, Fukusumi M. MWCNTs/AZ31 surface composites fabricated by friction stir processing. Mater Sci Eng, A 2006;419:344–8.
[23] Ratna Sunil B, Sampath Kumar TS, Chakkingal Uday, Nandakumar V, Doble Mukesh. Friction stir processing of magnesium–nanohydroxyapatite composites with controlled in vitro degradation behavior. Mater Sci Eng C 2014;39:315–24.
[24] Azizieh M, Larki AN, Tahmasebi M, Bavi M, Alizadeh E, Kim HS. Wear behavior of AZ31/Al2O3 magnesium matrix surface nanocomposite fabricated via friction stir processing. J Mater Eng Perform 2018;27:2010–7.
[25] Yousefpour Foroozan, Jamaati Roohollah, Aval Hamed Jamshidi. Synergistic effects of hybrid (HA+Ag) particles and friction stir processing in the design of a high-strength magnesium matrix bio-nano composite with an appropriate texture for biomedical applications. J Mech Behav Biomed Mater 2022;125:104983.
[26] Eivani AR, Mehdizade M, Ghosh M, Jafarian HR. The effect of multi-pass friction stir processing on microstructure, mechanical properties, and corrosion behavior of WE43-nHA bio-composite. J Mater Res Technol 2023;22:776–94.
[27] Zhang Weiwei, Li Baosong, Hong Ming, Li Mingyuan. Effects of cerium oxide doping on microstructure and properties of Ni-GO-CeO2 nanocomposite coatings. J Mater Res Technol 2022;21:3440–50.
[28] Aydin Fatih, Durgut Rafet, Mustu Mustafa, Demir Bilge. Prediction of wear performance of ZK60/CeO2 composites using machine learning models. Tribol Int 2023;177:107945.
[29] Chang CI, Wang YN, Pei HR, Lee CJ, Du XH, Huang JC. Microstructure and mechanical properties of nano-ZrO2 and nano-SiO2 particulate reinforced AZ31-Mg based composites fabricated by friction stir processing. Key Eng Mater 2007;351:114–9.
[30] Paidar Moslem, Ojo Olatunji Oladimeji, Ezatpour Hamid Reza, Akbar Heidarzadeh. Influence of multi-pass FSP on the microstructure, mechanical properties and tribological characterization of Al/B4C composite fabricated by accumulative roll bonding (ARB). Surf Coating Technol 2019;361:159–69.
[31] Liu Fenjun, Li Aodong, Shen Zhikang, Chen Haiyan, Yan Ji. Microstructure and corrosion behavior of Al-Ti-TiC-CNTs/AZ31 magnesium matrix composites prepared using laser cladding and high speed friction stir processing. Opt Laser Technol 2022;152:108078.
[32] Sharma Sanjay, Amit Handa, Singh Sahib Sartaj, Verma Deepak. Influence of tool rotation speeds on mechanical and morphological properties of friction stir processed nano hybrid composite of MWCNT-Graphene-AZ31 magnesium. J Magnesium Alloys 2019;7:487–500.
[33] Liu Shoufa, Zhang Shaoguo, Vaira Vignesh R, Ojo Olatunji Oladimeji, Mehrez Sadok, Mohanavel Vinayagam, Paidar Moslem. Probe-less friction stir spot processing (PFSSP) of AA5754/AA5083 joint by adding the B4C ceramics: effect of shoulder features on mechanical properties and tribological behavior. Vacuum 2023;207:111542.
[34] Liu Shoufa, Paidar Moslem, Mehrez Sadok, Ojo Olatunji Oladimeji, Mahariq Ibrahim, Elbadawy Ibrahim. Development of AA6061/316 stainless steel surface composites via friction stir processing: effect of tool rotational speed. Mater Char 2022;192:112215.
[35] Paidar Moslem, Ali Asgari, Ojo Olatunji Oladimeji, Saberi Abbas. Mechanical properties and wear behavior of AA5182/WC nanocomposite fabricated by friction stir welding at different tool traverse speeds. J Mater Eng Perform 2018.
[36] Ma Wenming, Ojo Olatunji Oladimeji, Paidar Moslem, Mehrez Sadok, Mohd Zain Azlan, Kulandaivel Arul. Improving the wear resistance and mechanical properties of hybridized AZ80 Mg/CeO_2+ZrO_2 surface composite by friction stir processing: effect of pin geometry. Vacuum 2023;212:111980.
[37] Dinaharan Isaac, Zhang Shuai, Chen Gaoqiang, Shi Qingyu. Titanium particulate reinforced AZ31 magnesium matrix composites with improved ductility prepared using friction stir processing. Mater Sci Eng, A 2020;772:138793.

[38] Ali Moharrami, Ahmad Razaghian, Paidar Moslem, Slapakova Michaela, Ojo Olatunji Oladimeji, Taghiabadi Reza. Enhancing the mechanical and tribological properties of Mg2Si-rich aluminum alloys by multi-pass friction stir processing. Mater Chem Phys 2020;250:123066.

[39] Amra M, Ranjbar Khalil, Hosseini SA. Microstructure and wear performance of Al5083/CeO_2/SiC mono and hybrid surface composites fabricated by friction stir processing. Trans Nonferrous Metals Soc China 2018;28:866–78.

[40] Maji Pabitra, Nath Rahul Kanti, Pritam Paul RK. Bhogendro Meitei, Subrata Kumar Ghosh, Effect of processing speed on wear and corrosion behavior of novel MoS2 and CeO2 reinforced hybrid aluminum matrix composites fabricated by friction stir processing. J Manuf Process 2021;69:1–11.

[41] Patel V, Li W, Andersson J, Li N. Enhancing grain refinement and corrosion behavior in AZ31B magnesium alloy via stationary shoulder friction stir processing. J Mater Res Technol 2022;17:3150–6.

[42] Zhang Mingming, Paidar Moslem, Ojo Olatunji Oladimeji, Mehrez Sadok, Narayanasamy Stalin, Mohd Zain Azlan, Mohanavel Vinayagam. Impact of multiple FSP passes on structure, mechanical, tribological and corrosion behaviors of AA6061/316 stainless-steel reinforced Al matrix composites. Surf Coating Technol 2022;447:128801.

[43] Liu Shoufa, Paidar Moslem, Ojo Olatunji Oladimeji, Poková Michaela Šlapáková, Mehrez Sadok, Mohd Zain Azlan, Zhao Qiaorong, Wang Jinpeng. Friction stir processing of hybridized AZ31B magnesium alloy-based composites by adding CeO2 and ZrO_2 powders: mechanical, wear, and corrosion behaviors. J Mater Res Technol 2023;24:1949–72.

[44] Li Hui, Paidar Moslem, Ojo Olatunji Oladimeji, Vaira Vignesh R, Iswandi Iswandi, Mehrez Sadok, Mohd Zain Azlan, Mohanavel V. Effect of tool profile on wear and mechanical behaviors of CeO_2 and ZrO_2-reinforced hybrid magnesium matrix composite developed via FSP technique. J Manuf Process 2023;94:297–315.